

## Article

# Frequency Containment Control of Hydropower Plants Using Different Adaptive Methods

Doğan Gezer <sup>1,\*</sup> , Yiğit Taşcıoğlu <sup>2</sup> and Kutay Çelebioğlu <sup>3</sup><sup>1</sup> TUBITAK MRC Energy Institute, METU Campus, Ankara 06531, Turkey<sup>2</sup> Department of Mechanical Engineering, TED University, Ankara 06420, Turkey; yigit.tascioglu@tedu.edu.tr<sup>3</sup> TOBB University of Economics and Technology, ETU Hydro, Ankara 06560, Turkey; kutaycelebioglu@gmail.com

\* Correspondence: dogan.gezer@tubitak.gov.tr; Tel.: +90-312-210-1830

**Abstract:** With the growth in the share of variable renewable energy sources, fluctuations in the power generation caused by these types of power plants can diminish the stability and flexibility of the grid. These two can be enhanced by applying frequency containment using hydropower plants as an operational reserve. The frequency containment in hydropower plants is automatically controlled by speed governors within seconds. Disturbances such as fluctuations in the net head and aging may diminish the performance of the controllers of the speed governors. In this study, model reference adaptive control approaches based on the Massachusetts Institute of Technology (MIT) rule and Lyapunov method were exploited in order to improve the performance of the speed governor for frequency containment control. The active power control with frequency control was enhanced by the aforementioned adaptive control methods. A mathematical model of a hydropower plant with a surge tank and medium penstock was constructed and validated through site measurements of a plant. It was shown that, as they are applicable in real life, both methods perform significantly better compared to conventional proportional-integrator control. Even in first five deviations, the performance of the conventional controller improved by 58.8% using the MIT rule and by 65.9% using the Lyapunov method. When the two adaptive control approaches were compared with each other, the MIT rule outputted better results than the Lyapunov method when the disturbance frequency was higher; however, the latter was more functional for rare disturbances.

**Keywords:** frequency containment control; hydropower plant; Lyapunov stability; MIT rule; model reference adaptive control; speed governor



**Citation:** Gezer, D.; Taşcıoğlu, Y.; Çelebioğlu, K. Frequency Containment Control of Hydropower Plants Using Different Adaptive Methods. *Energies* **2021**, *14*, 2082. <https://doi.org/10.3390/en14082082>

Academic Editor: Sebastian Muntean

Received: 13 February 2021

Accepted: 7 April 2021

Published: 8 April 2021

**Publisher's Note:** MDPI stays neutral with regard to jurisdictional claims in published maps and institutional affiliations.



**Copyright:** © 2021 by the authors. Licensee MDPI, Basel, Switzerland. This article is an open access article distributed under the terms and conditions of the Creative Commons Attribution (CC BY) license (<https://creativecommons.org/licenses/by/4.0/>).

## 1. Introduction

As the penetration of variable renewable energy sources (V-RES) such as wind and photovoltaics in the grid increases to higher proportions, a higher amount of operational reserve will be needed to provide grid stability and flexibility. Grid stability involves the availability of electricity at all times and a power quality covering the voltage and frequency stability. In a similar manner, grid flexibility means the capacity for load and generation fluctuations, especially resulting from the high share of V-RESs. The operation of hydropower plants (HPPs) with storage capacity (e.g., reservoir HPPs) is a key solution for maintaining the power quality and grid flexibility of an interconnected network, relying on their very short start-up and action times.

Considering the frequency stability, there are four steps of action that can be taken against the frequency deviation [1]. The most rapid one is frequency containment control (FCC), formerly known as primary frequency control, which is used for limiting the deviations in the grid frequency within a few seconds. These deviations result from the imbalance between demand (e.g., load fluctuations) and supply (e.g., intermittent generation of V-RESs). The units contributing to the frequency containment control automatically start this action. In HPPs, the speed governor of the unit is responsible for the FCC. Speed

governors adjust the turbine speed for grid synchronization. Following the synchronization process, the speed governors regulate the active power output for network operation. As long as the FCC function is on, they are expected to increase/decrease the active power output of the unit depending on the sign of the frequency deviation, i.e., an increase in the frequency, meaning an excess of supply, will result in the automatic action of speed governors by decreasing the active power. As there exist other generating units contributing to the frequency response, each unit takes a portion of the required load according to its permanent speed droop value. An FCC action is traditionally implemented at the generation side in the existing control strategy of the speed governors. Recent studies on FCC have focused on the high penetration of V-RESs. Flywheel systems for inertia control were proposed in [2] for active power support in the case of frequency dips. A fuzzy-logic-based algorithm controls the bidirectional active power flow in a wind farm, according to the system frequency and the rate-of-change of system frequency. The possibility of FCC in smaller-alternative-current (AC) subnetworks that are connected to a high-voltage direct current (HVDC) network was investigated [3]. Different controller schemes were analyzed to benefit from the abundant inertial resources of rotors in wind power plants [4]. FCC studies for HPPs have concentrated on performance analyses of HPP models with/without surge tanks in [5,6] using frequency response, step response, and setpoint change tests.

The state of the art for hydraulic turbine control is digital governors, mostly with Proportional—Integral (PI) controllers and some with modern control techniques [7]. These controllers are tuned under ideal conditions with newly installed equipment. On the classical control side, PI control stability issues [8,9] and techniques for tuning PI parameters [10–13] have been studied by the majority. On the modern control side, various studies have covered nonlinear, optimal, and robust control using state variable representation. A self-tuning power system stabilizer, which uses the minimization of the quadratic performance index, was presented in [14]. A genetic algorithm was used in [15] to optimize the speed governor performance of an HPP. Speed governor designs with neural networks were described in [16] with an intelligent PI tuning method, in [17] for an isolated power system, and in [18] by the implementation of neuro-controllers. The robust control of hydraulic turbines through frequency-response was presented in [19]. In [20], a robust  $H_\infty$  control was investigated for a very long headrace tunnel. Ref. [21] studied the multi-frequency dynamic performance of an HPP with a surge tank through the coupling effect among penstock, a water turbine, and the electrical grid. In [22], the chaotic motion of the speed governor was investigated while nonlinear turbine characteristics were present.

The performance of speed governors can be disrupted by the changes in the reservoir and tailwater levels, as well as aging effects, e.g., wear and tear in the flow-regulating mechanism. Model reference adaptive control (MRAC) can improve the performance of speed governors in the presence of these disturbances, as MRAC with the Massachusetts Institute of Technology (MIT) rule and Lyapunov method follows the desired behavior described by a reference model.

MRAC for FCC is only investigated in [23] for micro-grids. However, there is a gap in the literature for MRAC usage for FCC in interconnected networks.

In this study, the usage of MRAC for FCC in an interconnected grid was investigated. First, a dynamic HPP model and a reference model describing the ideal behavior for FCC were formed. Then, adaptive controllers, designed with the MIT rule and the Lyapunov method, were added into the main active power control loop of the speed governor to rapidly adapt the controller to the changing plant conditions. Finally, the simulation results of both controllers were compared.

The rest of the article is organized as follows: the HPP modeling is detailed in Section 2. The proposed controllers including the MIT rule and the Lyapunov method, along with the reference model, are presented in Section 3. The simulations and results are presented in Section 4, and Section 5 concludes the paper.

## 2. Hydropower Models

The control parameters of speed governors are traditionally determined by using linear models. This approach is convenient when the changes in the loading and speed of the unit are within 10% and 1%, respectively.

On the other hand, significant changes in the active power output and turbine speed of the unit occur during isolated (i.e., without being interconnected with other generating units) or islanded (i.e., interconnection with only a small number of units) operation, as well as during loading, unloading, load rejection, and turbine speed adjustment before network synchronization. It is necessary to simulate the speed governor controller and related systems with nonlinear models for changes larger than 25% in loading and 8% in turbine speed [24]. Nonlinear HPP models include the compressibility of water. An instance of this effect could be the propagating wave and hydraulic pressure oscillations in penstock during load rejections [25].

In this study, a nonlinear model was used to test all possible scenarios and a linear model was used to conduct a stability analysis of the controller. Figure 1 shows the general layout of an HPP including the feedbacks to the speed governor.

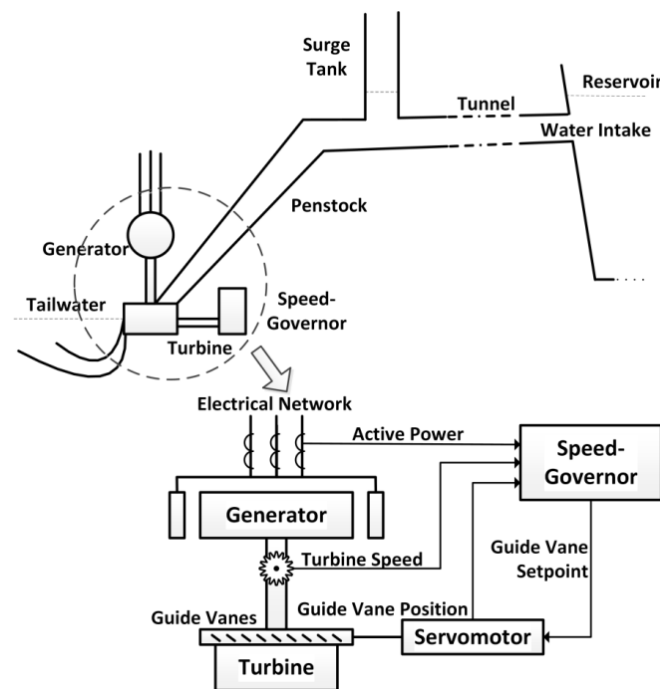


**Figure 1.** General layout of a hydropower plant (HPP).

### 2.1. Nonlinear HPP Model

The modeling equations of the depicted components in the waterway, servomotor and guide vanes, turbine, and generator are given in the following subsections [24–32]. Many of the quantities below are given in the per-unit system, which is the expression of the quantities as a ratio of the actual value over the base value, and it is dimensionless. The base value is the rated value of the quantity during normal operation.

#### 2.1.1. Waterway (Tunnel, Surge Tank, and Penstock)

The relationships between the water head in the turbine and the reservoir level, including the energy tunnel, surge tank, penstock dynamics, and friction loss, are given as follows:

### Tunnel

The rate of change of water velocity through the tunnel is calculated as:

$$\frac{dU_{wt}}{dt} = \frac{H_r - H_s - H_{ft}}{t_{wt}} \quad (1)$$

where  $U_{wt}$  is the water velocity through the tunnel in pu,  $H_r$  is the reservoir water level in pu,  $H_s$  is the water level in the surge tank in pu,  $H_{ft}$  is the head loss due to friction in the tunnel in pu, and  $t_{wt}$  is the water starting time of the tunnel in s, which is calculated as:

$$t_{wt} = \frac{Q_0}{H_0 g} \sum \frac{l_t}{A_t} \quad (2)$$

where  $Q_0$  is the nominal flow rate in  $\text{m}^3/\text{s}$ ,  $H_0$  is the nominal net head in m,  $g$  is the gravitational acceleration in  $\text{m}^2/\text{s}$ , and  $l_t$  and  $A_t$  are the length and cross-sectional area of tunnel portions in m and  $\text{m}^2$ , respectively.

### Surge Tank

The water level in the surge tank is found as:

$$H_s = \frac{1}{C_s} \cdot \int (U_{wt} - U_{wp}) \cdot dt \quad (3)$$

where  $C_s$  is the storage capacity of the surge tank in s, and  $U_{wt}$  and  $U_{wp}$  are the water velocities, in pu, through the tunnel and penstock, respectively. The storage capacity is calculated as follows:

$$C_s = \frac{A_s H_0}{Q_0} \quad (4)$$

where  $A_s$  is the average cross-sectional area of the surge tank in  $\text{m}^2$ .

### Penstock

The rate of change of water velocity through the penstock is defined as:

$$\frac{dU_{wp}}{dt} = \frac{H_s - H_{tur} - H_{fp} - H_w}{t_{wp}} \quad (5)$$

where  $H_{tur}$  is the water head in the turbine in pu,  $H_{fp}$  is the head loss due to friction in the penstock in pu,  $H_w$  is the head change due to the propagating wave effect in pu, and  $t_{wp}$  is the water starting time of the penstock in s, which is calculated as follows:

$$t_{wp} = \frac{Q_0}{H_0 g} \sum \frac{l_p}{A_p} \quad (6)$$

where  $Q_0$  is nominal flow rate in  $\text{m}^3/\text{s}$ ,  $H_0$  is the nominal net head in m,  $g$  is the gravitational acceleration in  $\text{m}^2/\text{s}$ , and  $l_p$  and  $A_p$  are the length and cross-sectional area of penstock portions in m and  $\text{m}^2$ , respectively.

The water starting time or water time constant is the time needed to accelerate the water in the penstock from zero discharge to the rated discharge under the rated head. This parameter is used in both linear and nonlinear models. Its value depends on the length and cross-sectional area of the penstock, rated head, and discharge.

#### 2.1.2. Turbine and Servo Cylinders

The relationships between the mechanical power output of the turbine and the guide vane opening, including the servo cylinder and the water head in front of the turbine, are given below:

The mechanical power output of the turbine is defined as follows:

$$P_m = K_{tur} \cdot H_{tur} \cdot (U_{tur} - U_{nl}) = T_m \cdot \omega \quad (7)$$

where  $P_m$  is the mechanical power output of the turbine in pu,  $K_{tur}$  is the turbine gain,  $H_{tur}$  is the water head in front of the turbine in pu,  $U_{tur}$  and  $U_{nl}$  are the water velocities, in pu, through the turbine at load and no-load, respectively,  $T_m$  is the mechanical torque in pu, and  $\omega$  is the turbine speed in pu.

$U_{tur}$  depends on  $H_{tur}$  and the guide vane opening  $G$ , and it is equal to  $U_{wp}$ :

$$U_{tur} = U_{wp} = G\sqrt{H_{tur}} \quad (8)$$

The turbine gain,  $K_{tur}$ , is defined as:

$$K_{tur} = \frac{1}{G_{fl} - G_{nl}} \quad (9)$$

where  $G_{fl}$  and  $G_{nl}$  are, respectively, the full-load and no-load of the guide vane openings.

$$\frac{dG}{dt} = \frac{1}{t_{servo}} (G_{set} - G) e^{-st_{del\_ser}} \quad (10)$$

where  $G$  is the guide vane opening in pu,  $t_{servo}$  is the time constant of the servomotor in s,  $G_{set}$  is the guide vane opening setpoint, in pu, sent from the speed governor controller, and  $t_{del\_ser}$  is the time delay for servo opening in s.

### 2.1.3. Generator and Excitation System

The equations relating the turbine speed with the electrical torque, including field voltage, are given as follows:

$$2H \frac{d\omega}{dt} = T_m - T_e \quad (11)$$

where  $T_e$  is the electromagnetic torque in pu, and  $H$  is the inertia constant, in s, which depends on the flywheel effect [29] as:

$$H = \frac{1}{2} \left( \frac{\pi}{60} \right)^2 \frac{GD^2 n^2}{S} \quad (12)$$

where  $GD^2$  is the flywheel effect of the generator in  $\text{tone.m}^2$ ,  $n$  is the turbine speed in rpm, and  $S$  is the nominal apparent power of the generator in kVA.

The generator in the steady-state is electrically modeled by considering the simplifications explained in [30]:

$$P_e = \frac{|E_q| |V_s|}{X_d + X_e} \sin \delta \quad (13)$$

where  $E_q$  is the generator internal voltage in pu,  $V_s$  is the voltage of the electrical network bus in pu,  $\delta$  is the angle between  $E_q \angle \delta^\circ$  and  $V_s \angle 0^\circ$ ,  $X_d$  is the direct axis reactance in pu,  $X_e$  is the bus impedance in pu, and:

$$E_q = \frac{n M_f V_f}{r_f} \quad (14)$$

where  $V_f$  is the main field voltage in pu,  $M_f$  is the mutual inductance between the field and any armature phase in pu, and  $r_f$  is the resistance of the field circuit in pu.

The interactions between the subsystems of the generic model are depicted in Figure 2. The implementation of the generic nonlinear model is given in Figure 3.

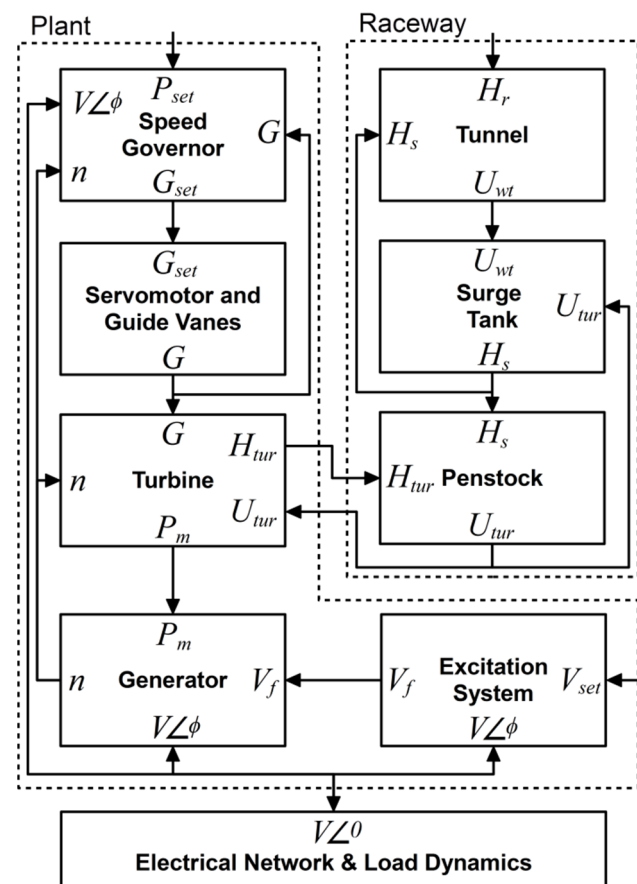


Figure 2. The interactions between subsystems in an HPP.

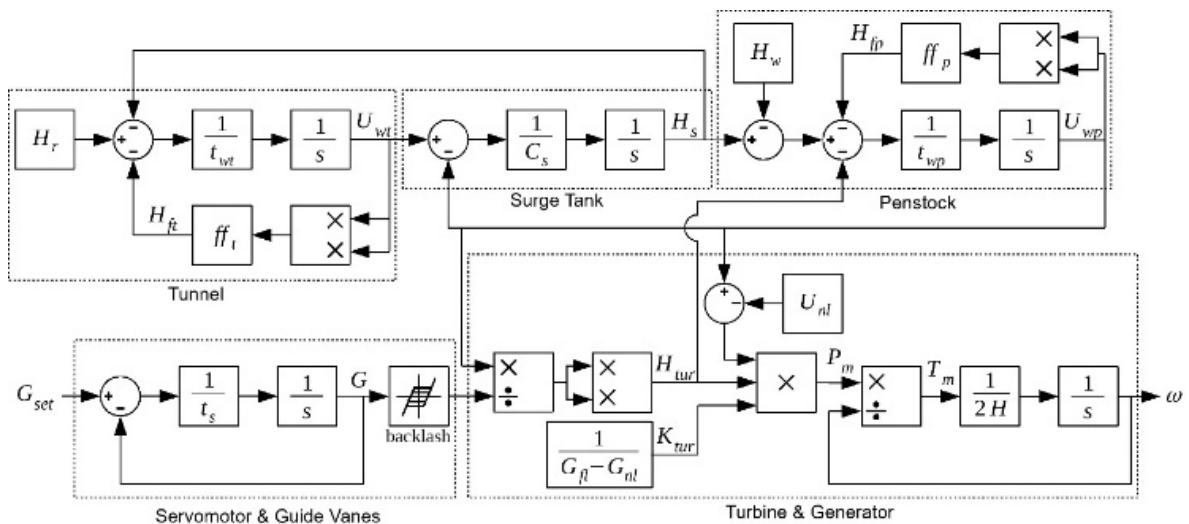


Figure 3. The schematic of the mathematical model implementation.

### 2.2. Linear HPP Model

Linear models are used for modeling small changes in the turbine speed and the active power of the HPP. Stability issues for the controller are investigated through the linear model. Linear model equations are obtained by the linearization of the aforementioned nonlinear equations around an operating point. The linearization of relationships between the mechanical power output of the turbine, the head in front of the turbine, the velocity of the water entering the turbine, and the guide vane opening resulting from Equations (7) and

(8) result in a linear equation linking the mechanical power output of the turbine and the guide vane opening in Equation (15).

$$\frac{\Delta P_m}{\Delta G} = \frac{1 - t_{wp}s}{1 + \frac{1}{2}t_{wp}s} \quad (15)$$

where  $t_{wp}$  is the water starting time of the penstock in s.

When the natural frequency effect is taken into account, the dynamic behavior due to the presence of penstock and the surge tank is obtained as in Equation (16) [33].

$$\left. \begin{aligned} \frac{\Delta P_m}{\Delta G} &= \frac{s^2 - \omega_s^2 t_{wp}s + \omega_s^2}{s^2 + \frac{1}{2}\omega_s^2 t_{wp}s + \omega_s^2} \\ \omega_s &= \sqrt{\frac{gA_p}{l_p A_s}} \end{aligned} \right\} \quad (16)$$

where  $t_{wp}$  is the water starting time of the penstock in s and  $\omega_s$  is the natural frequency of the mass oscillation due to the surge tank in rad/s.  $\omega_s$  could be calculated by using  $l_p$  and  $A_p$ , which are the length and cross-sectional area of the penstock in m and  $m^2$ , respectively, and  $A_s$ , which is the cross-sectional area of the surge tank in  $m^2$ .

### 2.3. System Description

In this study, Seyhan I HPP was modeled with the characteristic parameters listed in Table 1. Seyhan I HPP is an aged hydropower plant that started operation in 1957. It has three vertical Francis turbines with 22.5 MVA of installed capacity each.

**Table 1.** Characteristic parameters of Seyhan I HPP.

Parameter	Value	Unit
Nominal net head	32	m
Nominal flow rate	77	$m^3/s$
Surge tank storage capacity	124.8	s
Surge tank cross-sectional area	380	$m^2$
Penstock length	81.7	m
Penstock cross-sectional area	21.2	$m^2$
Penstock friction factor	0.05	-
Guide vane opening at no-load	11	%
Guide vane opening at full-load	85	%
Servomotor time constant	4	s
Guide vane delay time	2	s
Flywheel effect of the generator	3320	tone. $m^2$
Turbine nominal speed	125	rpm
Apparent power of the generator	22.5	MVA
Inertia constant of the generator	3.14	s

A mathematical model of Seyhan I HPP is based on the following assumptions and modeling principles:

1. The modeled HPP has a short-medium penstock and a surge tank, but it does not have an energy tunnel. Although there are no common or standardized lengths to classify the penstocks, if any fluctuations in the active power output are observed due to wave effects within the penstock, the penstock can be considered as medium-long and the wave effect should be taken into account while modeling the waterway. Hence, wave propagation is not considered;
2. The electrical dynamics of the generator has a very short time constant compared to that of hydrodynamics [34]. Electromagnetic interactions in the generator occur much faster than the speed governor control actions do; hence, electromagnetic generator dynamics are not considered. On the other hand, during the adjustment of the turbine

speed before network synchronization, it is critical to pay regard to the mechanical starting time (also known as mechanical inertia time) for tuning speed governor parameters. Furthermore, the speed rise following a load rejection is limited by the rotational inertia of the unit. The turbine rotational inertia is approximately 5% of the generator rotational inertia [27], meaning that the rotational inertia of the unit dominantly depends on the generator characteristic rather than the hydraulic turbine. Therefore, the rotational inertia of the generator is taken into account;

3. The modelling of the electrical grid and load is necessary for simulations of the speed governor in isolated and islanded modes of operation, where small load changes result in significant frequency deviations. An interconnected mode of operation, as preferred in this study, requires the network frequency to be kept constant [35].

#### 2.4. Model Validation

As the validation methodology, the mathematical model was constructed considering the aforementioned assumptions and modeling principles. Then, site tests were conducted for unit start-up, shut-down, and loading. The guide vane opening, the turbine speed, and the active power measurements were recorded during the site tests. Following the site tests, the measured guide vane opening values were given as workspace inputs to the mathematical model in MATLAB/Simulink. The simulations conducted led to the simulated turbine speed and the simulated active power. These simulation results were compared with the actual site measurements in Figure 4a–c during start-up and shut-down, and the unit was disconnected from the grid. The simulated turbine speed profiles were in close agreement with the site measurements. In Figure 4b, the unit was already synchronized with the network; hence, the guide vane opening affected the active power output. Despite the acceptable lead in the simulated response, loading profiles were in correspondence, and they attained the same active power output.

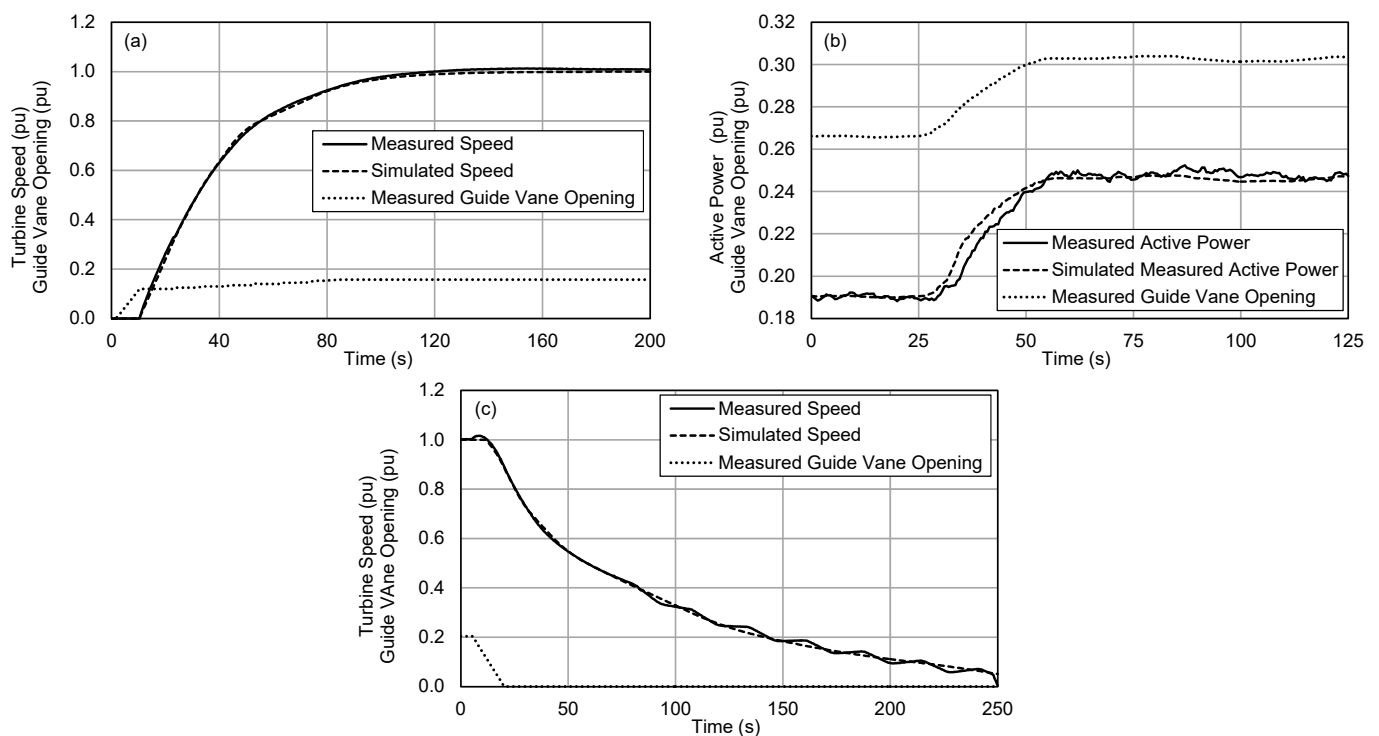


**Figure 4.** Model validation of Seyhan I HPP with site measurements during (a) start-up, (b) loading, and (c) shutdown.

In Figure 5, different models are compared with the measured active power. Each model was given the measured guide vane opening values as input. The first linear model was constructed by using the relationship in Equation (15). The second was established

using Equation (16). The third was the nonlinear model generated by Equations (1)–(14). Although the nonlinear model had the most correspondence, in order to use it in stability issues, the model by Equation (16) was the most convenient one.

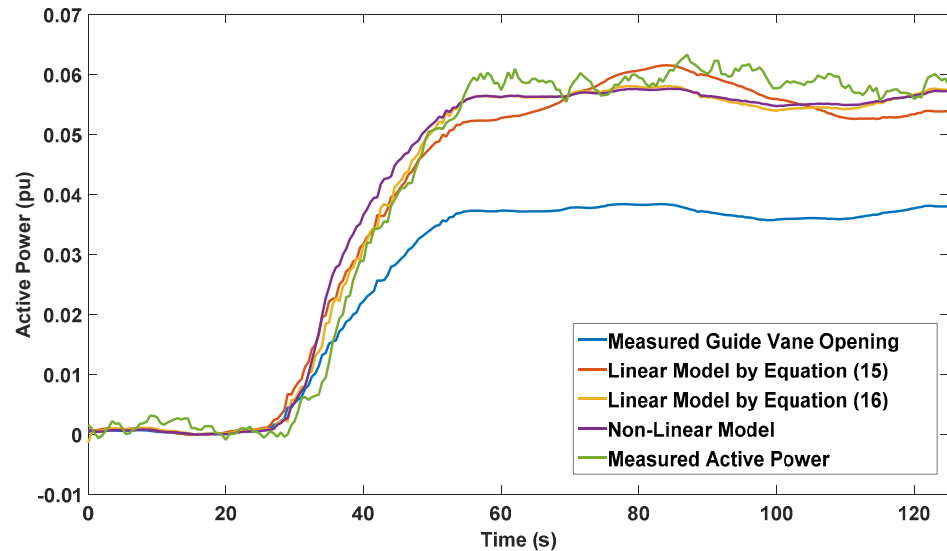


Figure 5. Comparison of various models with site measurements.

### 3. Proposed Adaptive Methods

Speed governors take advantage of active power control in order to follow the active power setpoint given by the operator. Figure 6 shows that the input of the main PI controller (with proportional gain,  $K_p$ , and the integral time,  $T_i$ ) has two branches with different setpoints and feedbacks. One is the active power control branch, where the error is the difference between the given active power setpoint,  $P_{set}$ , and the measured active power,  $P$ . The other is the FCC branch, through which the frequency deviation ( $f_{set} - f$ ) exceeding the speed dead-band is added to the active power control branch after being divided by the permanent speed droop,  $R$ . Figure 6 shows the inside of the speed governor in Figure 1.

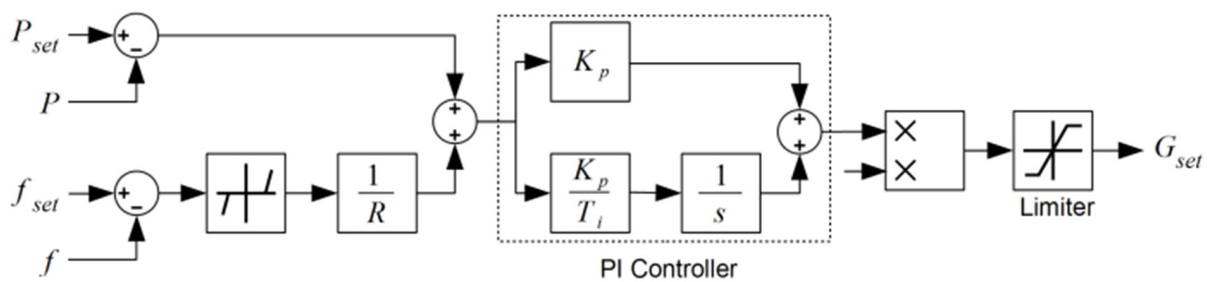
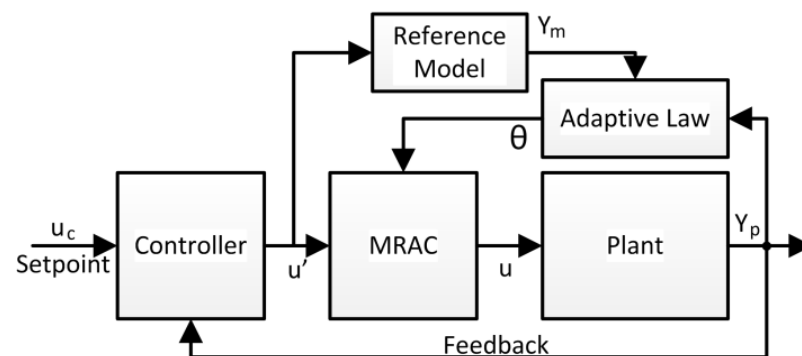


Figure 6. Active power control with frequency containment.

Adaptive control is used for the automatic adjustment of controllers in real-time to maintain the desired performance. It is an efficient technique for dealing with deviations and uncertainties in slow-varying plant parameters [36,37].

MRAC is a direct adaptive control approach, in which the desired performance of the plant controller is obtained through a dynamic model called the reference model. This controller has an ordinary feedback loop taken from the process and another loop for adjusting the controller parameters. As displayed in Figure 7, the controller—which outputs a processed setpoint through comparing the given setpoint and the feedback signal, the plant in which the process occurs, the reference model by which the desired performance of the plant is modeled, and the adaptation mechanism that compares the outputs of the reference model and the plant—and MRAC are the main parts in the adaptive

structure. The mechanism for adjusting the parameters can be developed by the gradient method (e.g., MIT rule) or stability theory (e.g., Lyapunov method).



**Figure 7.** General schematic for model reference adaptive control (MRAC).

### 3.1. Model Reference Adaptive Controller Using MIT Rule

The gradient design method is based on the MIT rule, which is used for the computation of approximate sensitivity functions. The adaptive law is designed such that the controller's parameters are tuned in a direction, which decreases the quadratic performance function. For this purpose, the partial derivative of the cost function is used. The output of the adaptation mechanism,  $\theta$ , and its relationship with the learning rate,  $\Gamma$ , the output of the reference model,  $Y_m$ , and the error,  $e$ , are written in Equation (17) [38,39].

$$\left. \begin{aligned} \text{Plant TF : } G_p &= \frac{y_p}{u} & \text{Model TF : } G_m &= \frac{y_m}{u'} \\ \text{Control Law : } u &= \theta u' \\ \text{Error : } e &= y_p - y_m \\ \text{Cost Function : } J(t, \theta) &= |e(t, \theta)|^2 \\ \text{MIT Rule : } \frac{d}{dt}\theta &= -\gamma \frac{\partial}{\partial \theta} J = -\gamma \left[ 2e \frac{\partial}{\partial \theta} e \right] \\ \theta &= -\Gamma \int [Y_m(t)e(t, \theta)dt] \end{aligned} \right\} \quad (17)$$

Figure 8 shows the block diagram of the proposed controller including MRAC with the MIT rule. In addition to the controller scheme shown in Figure 6, the reference model and adaptation mechanism are embedded. The frequency containment error is also given as an input to the reference model. A transport delay is added to represent the latency in the first movement of the guide vanes. The limiter in the reference model confines the reference model output in the predetermined active power reserve of the power plant. The difference between the ideal behavior through the reference model and the actual primary control action is given as an input to the adaptation mechanism. The output of the PI controller is corrected by the output  $\theta$  of the adaptation mechanism. In most speed governor systems, the output of the controller is limited by the load limiter. The controller output is sent to the guide vane mechanism actuator.

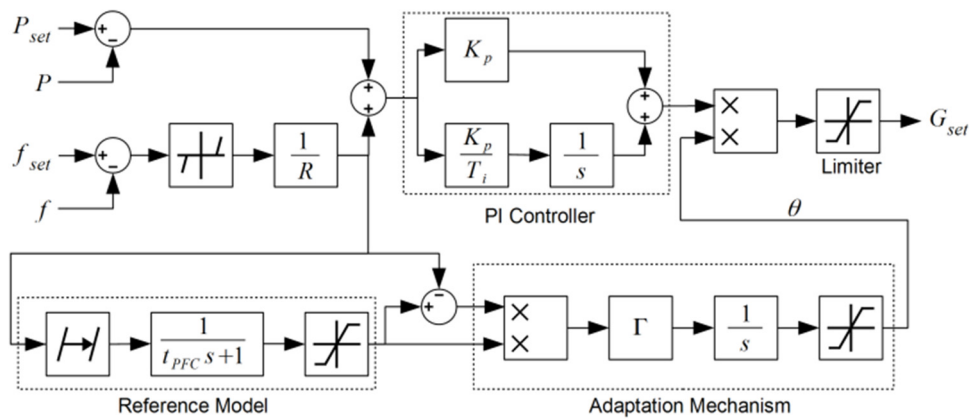


Figure 8. Block diagram of the controller with MIT rule.

### 3.2. Model Reference Adaptive Controller Using Lyapunov Method

The stability method relies on Lyapunov stability theory. This theory assures the stability and convergence of the error between the plant output and the model output. The procedure for developing the MRAC with the Lyapunov method starts with the derivation of the differential equation for the error. Then, a Lyapunov function is found that makes the error go to zero. In order to drive the error to zero, a Lyapunov function is used with a symmetric positive definite matrix P. The derivative of the Lyapunov function is made negative by solving the Lyapunov function with a positive definite matrix Q. The output of the adaptation mechanism,  $\theta$ , and its relationship with the learning rate,  $\Gamma$ , the output of the reference model,  $Y_m$ , and the error,  $e$ , are given in Equation (18) [40–42].

$$\left. \begin{aligned}
 \text{Plant TF : } G_p &= \frac{y_p}{u} & \text{Model TF : } G_m &= \frac{y_m}{u'} \\
 \text{Control Law : } u &= \theta u' \\
 \text{Error : } e &= y_p - y_m \\
 \text{Lyapunov Function : } V(x) &= x^T P x \\
 \text{Derivative : } \dot{V} &= \frac{1}{2} e^T(t) Q e(t) \\
 \theta &= -\Gamma \int [u'(t) e(t, \theta) dt]
 \end{aligned} \right\} \tag{18}$$

Figure 9 represents the block diagram for the model reference adaptive controller based on Lyapunov stability. The practical difference of this method compared to the MIT rule is using  $u'(t)$  instead of  $Y_m(t)$  as an input to the multiplication block within the adaptation mechanism.

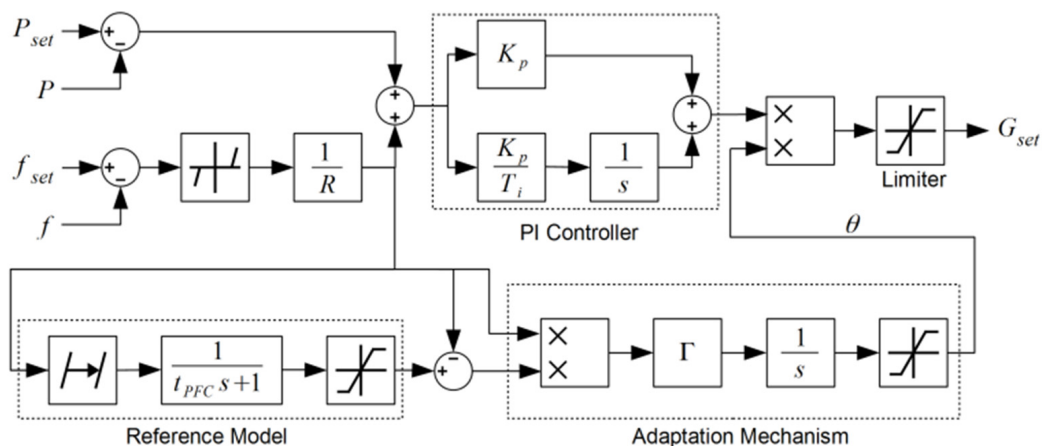


Figure 9. Block diagram of the controller with Lyapunov function.

### 3.3. Reference Model for Frequency Containment Control

Frequency containment control is the fastest control action taken against frequency deviations in the grid. All units, contributing to FCC, automatically give active power support by increasing/decreasing their active power output depending on the sign of the frequency deviation. An FCC action is expected to start immediately following the frequency deviation. All FCC reserves are to be given in 30 s and last for 15 min. In particular, hydropower plants are permitted to start this action with a 4 s delay at maximum [43,44].

As shown in Figure 10, the amount of active power contribution of each unit is determined according to the predefined permanent speed droop value. The responses of all interconnected units contributing to the FCC are coordinated with this value. The amount of active power support,  $\Delta P$ , of the unit depends on the amount of frequency deviation,  $\Delta f$ , and the permanent speed droop,  $R$ , i.e., a 200 mHz decrease in frequency of a 50 Hz network requires a 0.1 pu increase in active power output with a permanent speed droop of 0.04. The relationship between the frequency deviation, permanent droop, and change in active power output is given in Equation (19).

$$\Delta f = R \Delta P \quad (19)$$

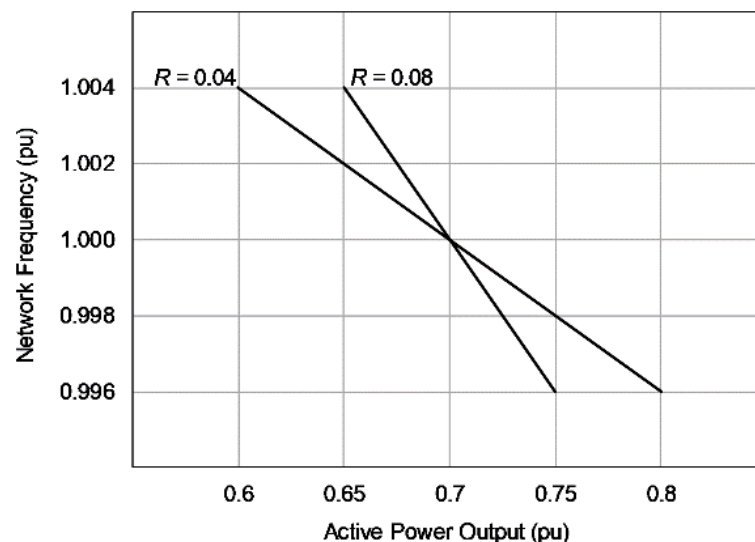


Figure 10. Change in active power output for different permanent speed droop values.

For the adaptive controller, a reference model is needed to define the desired behavior of the plant. A first-order transfer function, as given in Equation (20), is an appropriate reference model for the frequency containment action. A time constant,  $t_{PFC}$ , of 6 s is used in the simulations.

$$\frac{P_{model}}{f_{deviation}} = \frac{1}{t_{PFC}s + 1} \frac{1}{R} \quad (20)$$

The defined reference model with its permitted limits is depicted in Figure 11. Within 90 s after a negative frequency deviation, (e.g.,  $f = 49.8$  Hz), the actual control action should not exceed the ideal action by 2% of the nominal generator power output [45].

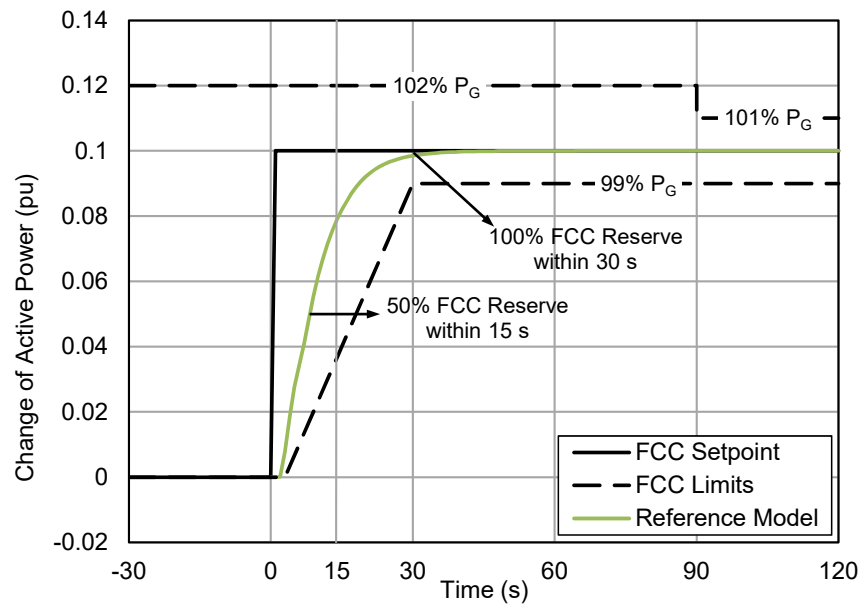


Figure 11. The step response of the reference model.

#### 4. Results

##### 4.1. Stability of the Power Control Loop

The parameters of the main PI controller shown in Figure 6 are  $K_p = 0.25$  and  $T_i = 11$  s. Figure 12 shows the root locus of the closed-loop system, with no active MRAC, for the different values of the proportional gain. The low-frequency pair of poles crosses to the right-hand side of the complex plane at  $K_p = 0.388$ . As the output of the MRAC effectively amplifies  $K_p$ , the closed-loop system is stable up to  $\theta = 1.55$ .

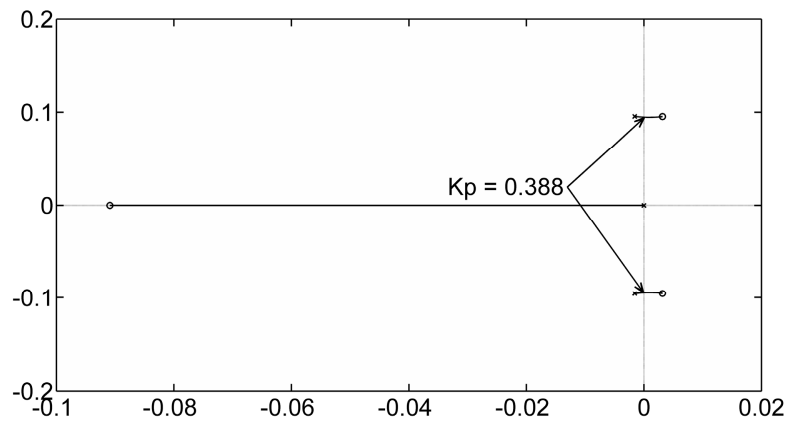


Figure 12. Root locus of the power control loop.

##### 4.2. Simulation Scenarios

###### 4.2.1. Change in Net Head

The reservoir level of an HPP could change from 0.9 pu, during an arid season, to 1.1 pu, following a rainy or snowy season. The presence of other units in the power plant, which are in operation, also raises the tailwater level or decreases the inlet pressure for a common penstock. The contribution of the MRAC for FCC is more perceivable when the net head drops to 0.9 pu. The speed governor opens the guide vanes more than that in the nominal head to reach the same active power output. This introduces latency in the FCC behavior. The  $H_r$  parameter is adjusted to reflect this scenario on the mathematical model.

#### 4.2.2. Degradation in Turbine Efficiency

The turbine efficiency could dramatically drop over the years due to aging. It is necessary to increase the guide vane opening to reach the same value of active power when the efficiency drops. This scenario could be simulated by increasing  $G_{fl}$ , which represents the guide vane opening at the nominal active power output. The increase in this parameter affects the turbine gain,  $K_{tur}$ .

#### 4.2.3. Deceleration in Guide Vane Driving

The elements in the guide vane driving system are the servo cylinder, hydraulic power unit, regulation ring, and the guide vanes. Any aging, clogging, and wear in this system could slow down the movement of the guide vanes. By changing the values of  $t_s$  and  $t_{del\_ser}$  parameters, this scenario will be reflected in the simulation.

#### 4.3. Simulation Results

Figure 13 shows the simulation results for the net head of 0.9 pu for the MRAC. The simulation conditions are as follows: The reference model matches the actual FCC action for the nominal head (i.e., net head of 1.0 pu). The learning rate,  $\Gamma$ , is 1 as long as the reference model corresponds to the actual FCC action. The permanent speed droop value,  $R$ , is 0.04. The FCC setpoint value changes between 0 and 0.1 as a result of the 0.004 pu frequency deviation, meaning a 49.8 Hz network frequency. Figure 13a displays the results for MRAC with the MIT rule; similarly, Figure 13b depicts the simulations for MRAC with the Lyapunov method. A pseudo-frequency deviation signal is given to the validated mathematical model. It is seen that when MRAC is not active, the action for FCC does not meet the requirements. It takes nearly 60 s to provide the necessary FCC reserve; however, it is expected to be given in 30 s. However, the FCC action satisfies the requirements as soon as MRAC is activated even when the  $\Gamma$  value is low with a very low number of occurrences (e.g., 0.8 after five cycles). As the number of the occurrences is increased to 50 and the  $\Gamma$  value is raised to 5, the FCC with the MIT rule action is nearly the same as the reference model. When focused on FCC with the Lyapunov method, it is seen that FCC with the Lyapunov method also satisfies the FCC requirements.

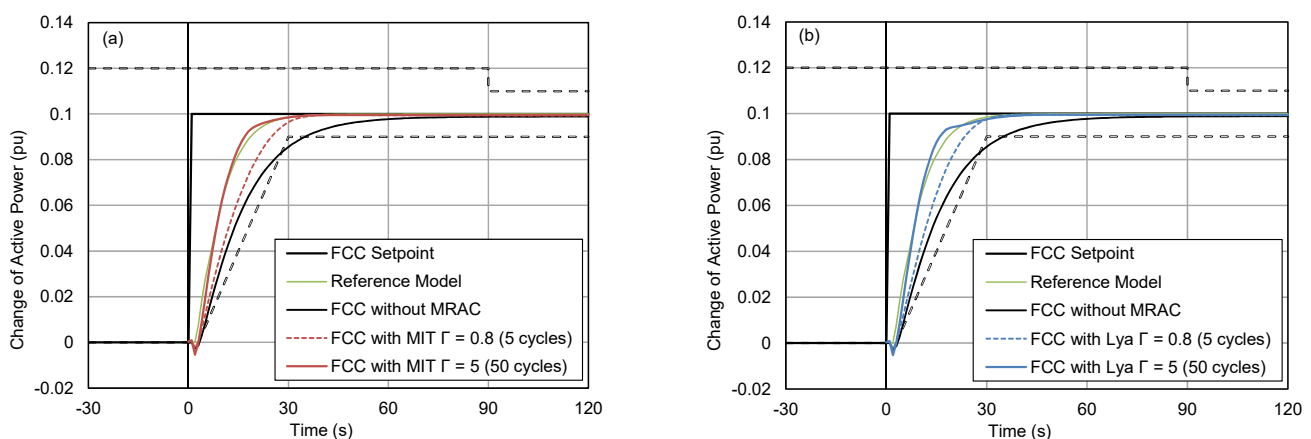


**Figure 13.** The FCC simulations for 0.9 pu net head: (a) MRAC with MIT rule; (b) MRAC with Lyapunov method.

The change in  $\theta$  for both the MIT rule and Lyapunov method is depicted in Figure 14. One should note that  $\theta$  converged to the same value and the convergence was faster with greater  $\Gamma$  values until a critical value. During the simulations, it was seen that when a critical  $\Gamma$  value was exceeded,  $\theta$  displayed unstable behavior. The critical  $\Gamma$  value was found to be 5.6 for MRAC with the MIT rule; similarly, the critical  $\Gamma$  value was found to be 7.1 for MRAC with the Lyapunov method. For the MRAC with the MIT rule, the  $\theta$  value converged to 1.15 independent of the value of the learning rate,  $\Gamma$ . For the MRAC with the Lyapunov method, the  $\theta$  value converged to 1.45. Considering these saturation values,

both MRAC controllers were within the stability margin, as explained in the previous section. However, a greater  $\theta$  value means a greater change in guide vane opening. As the  $\theta$  value was greater in the Lyapunov method, it is critical to limit the guide vane opening for secure operation.

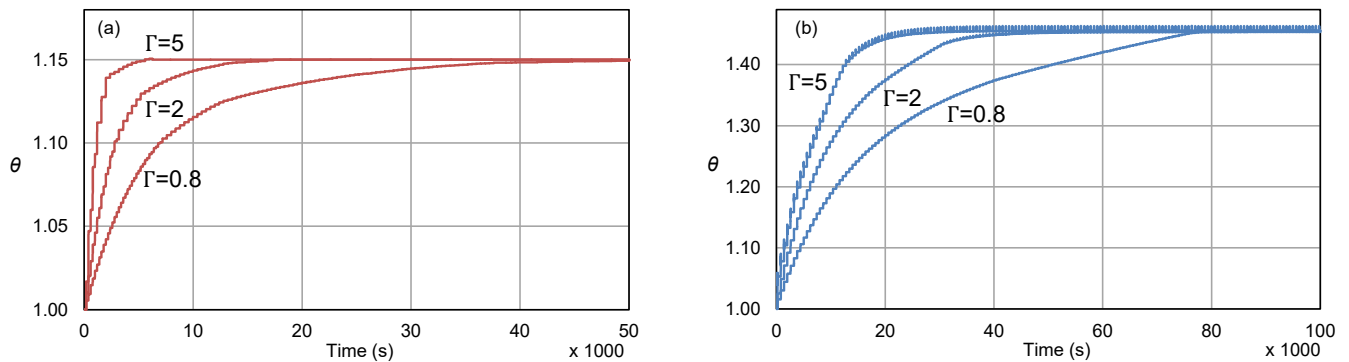


**Figure 14.** Change in  $\theta$  for (a) MRAC with the MIT rule and (b) MRAC with the Lyapunov method.

The insufficient response, i.e., when the MRAC was off, was set as the baseline performance for both the MIT rule and the Lyapunov method. The results of the simulations with different  $\Gamma$  values and the number of cycles for both methods (i.e., recursive occurrences of frequency deviation) are displayed on Figure 15 and listed in Table 2. The sum of the squared errors ( $e^2$ ) to the response of the reference model was normalized to 1 pu. After 5 cycles with  $\Gamma = 0.8$ , the improvement was 58.8% for the MIT rule and was 65.9% for the Lyapunov method. This shows that for the same number of occurrences and the learning rate, the Lyapunov method had a better improvement in performance. Similarly, after 50 cycles with  $\Gamma = 5$ , the improvement was 97.5% for the MIT rule and was 96.5% for the Lyapunov method. Considering the top performance, the MIT rule performed better than the Lyapunov method.

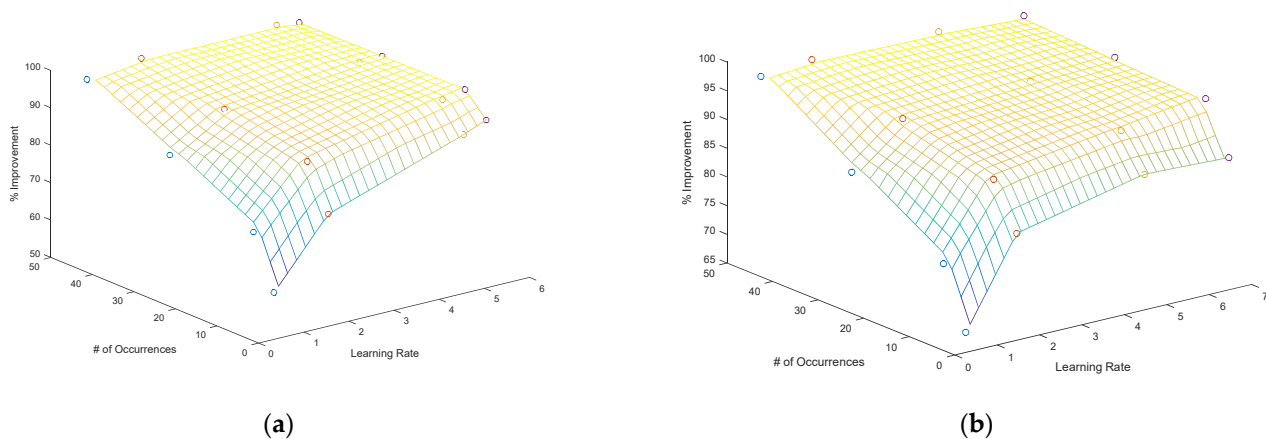


**Figure 15.** Performance index as a function of  $\Gamma$  and # of cycles: (a) MRAC with MIT rule; (b) MRAC with Lyapunov method.

**Table 2.** Results for the contribution of MRAC controllers.

Case		Number of Cycles	$\Sigma e^2$	Improvement wrt Baseline
Type	$\Gamma$			
MIT rule	-	-	1 pu	baseline
MIT rule	0.8	5	0.412 pu	58.8%
MIT rule	0.8	10	0.272 pu	72.8%
MIT rule	0.8	50	0.047 pu	95.3%
MIT rule	2	5	0.237 pu	76.3%
MIT rule	2	10	0.118 pu	88.2%
MIT rule	2	50	0.026 pu	97.4%
MIT rule	5	5	0.112 pu	88.8%
MIT rule	5	10	0.041 pu	95.9%
MIT rule	5	50	0.025 pu	97.5%
Lyapunov	0.8	5	0.341 pu	65.9%
Lyapunov	0.8	10	0.237 pu	76.3%
Lyapunov	0.8	50	0.039 pu	96.1%
Lyapunov	2	5	0.189 pu	81.1%
Lyapunov	2	10	0.111 pu	88.9%
Lyapunov	2	50	0.031 pu	96.9%
Lyapunov	5	5	0.139 pu	86.1%
Lyapunov	5	10	0.079 pu	92.1%
Lyapunov	5	50	0.035 pu	96.5%

## 5. Conclusions

Hydropower generation plays a crucial role in modern electric power systems to retard fluctuations caused by V-RESs. The FCC contribution of HPPs helps in decreasing the imbalances between supply and demand for the whole grid. In this study, model reference adaptive controllers with the MIT rule and Lyapunov method were designed for the speed governor controller of an HPP to improve the FCC performance of the unit.

The very first conclusion is that the performance of the conventional PI controller can be diminished by external disturbances, as shown in the simulations. Therefore, it is useful to add precautionary loops into the controller in order to provide the tuned performance. Secondly, adaptive controllers are very helpful in real life because it is not necessary to adjust adaptive parameters each time the disturbance occurs; however, the very first tuning of the adaptive controllers' parameters requires considerable experience or a high level of modeling. As the third conclusion, the MRAC with both the MIT rule and Lyapunov method in the active power control loop makes considerable improvements in FCC against slow-varying disturbances such as variations in the net head. Both adaptive methods are also convenient to implement on the off-the-shelf controllers such as programmable logical controllers (PLCs).

The final conclusion is on the comparison of the adaptive approaches. It was seen that the Lyapunov method has a better performance for a small number of occurrences (1–5 times); however, disregarding the time scales, the top performance of the MIT rule was greater than the Lyapunov method. For the same number of occurrences, the  $\theta$  value of the Lyapunov method reaches higher than the MIT rule, meaning that the guide vanes will be opened more in the Lyapunov method. This can bring a practical precaution of adding a limiter for this potential risk.

**Author Contributions:** Conceptualization, D.G., Y.T. and K.Ç.; methodology, D.G., Y.T. and K.Ç.; software, D.G.; validation, D.G.; formal analysis, D.G. and Y.T.; investigation, D.G.; resources, D.G.; data curation, D.G. and Y.T.; writing—original draft preparation, D.G., Y.T. and K.Ç.; writing—review and editing, D.G., Y.T. and K.Ç.; visualization, D.G. and Y.T.; supervision, Y.T. and K.Ç.; project administration, D.G. All authors have read and agreed to the published version of the manuscript.

**Funding:** This research received no external funding.

**Institutional Review Board Statement:** Not applicable.

**Informed Consent Statement:** Not applicable.

**Data Availability Statement:** The data presented in this study are available on request from the corresponding author.

**Acknowledgments:** The authors gratefully acknowledge the contributions of TUBITAK MRC through supporting this research study by the project “Seyhan I HPP Rehabilitation Project” numbered 5132804 and conducted at TUBITAK, Scientific and Technological Research Council of Turkey, Marmara Research Center (MRC) Energy Institute.

**Conflicts of Interest:** The authors declare no conflict of interest.

## References

1. European Network of Transmission System Operators for Electricity, ENTSOE. Available online: [https://www.entsoe.eu/fileadmin/user\\_upload/\\_library/news/ENTSO-Stakeholder\\_Workshop\\_LFC\\_\\_RNC\\_on\\_12\\_July/120606\\_Operational\\_Reserves\\_Report\\_public.pdf](https://www.entsoe.eu/fileadmin/user_upload/_library/news/ENTSO-Stakeholder_Workshop_LFC__RNC_on_12_July/120606_Operational_Reserves_Report_public.pdf) (accessed on 8 November 2018).
2. Jauch, C.; Hippel, S. Hydraulic–pneumatic flywheel system in a wind turbine rotor for inertia control. *IET Renew. Power Gener.* **2016**, *10*, 33–41. [[CrossRef](#)]
3. Bianchi, F.D.; Domnguez-Garca, J.L. Coordinated frequency control using MT-HVDC grids with wind power plants. *IEEE Trans. Sustain. Energy* **2016**, *7*, 213–220. [[CrossRef](#)]
4. Wang-Hansen, M.; Josefsson, R.; Mehmedovic, H. Frequency Controlling Wind Power Modeling of Control Strategies. *IEEE Trans. Sustain. Energy* **2013**, *4*, 954–959. [[CrossRef](#)]
5. Yang, W.; Yang, J.; Guo, W.; Norrlund, P. Response Time for Primary Frequency Control of Hydroelectric Generating Unit. *Int. J. Electr. Power Energy Syst.* **2016**, *74*, 16–24. [[CrossRef](#)]
6. Saarinen, L.; Norrlund, P.; Lundin, U. Field Measurements and System Identification of Three Frequency Controlling Hydropower Plants. *IEEE Trans. Energy Convers.* **2015**, *30*, 1061–1068. [[CrossRef](#)]
7. Fasol, K.H. A short history of hydropower control. *IEEE Control Syst.* **2002**, *22*, 68–76. [[CrossRef](#)]
8. Hagihara, S.; Yokota, H.; Goda, K.; Isobe, K. Stability of a Hydraulic Turbine Generating Unit Controlled by P.I.D. Governor. *IEEE Trans. Power Appar. Syst.* **1979**, *PAS-98*, 2294–2298. [[CrossRef](#)]
9. Phi, D.T.; Bourque, E.J.; Thorne, D.H.; Hill, E.F. Analysis and Application of the Stability Limits of a Hydro-Generating Unit. *IEEE Trans. Power Appar. Syst.* **1981**, *PAS-100*, 3203–3212. [[CrossRef](#)]
10. Wozniak, L. A graphical approach to hydrogenerator governor tuning. *IEEE Trans. Energy Convers.* **1990**, *5*, 417–421. [[CrossRef](#)]
11. Kamwa, I.; Lefebvre, D.; Loud, L. Small signal analysis of hydro-turbine governors in large interconnected power plants. In Proceedings of the 2002 IEEE Power Engineering Society Winter Meeting. Conference Proceedings (Cat. No.02CH37309), New York, NY, USA, 27–31 January 2002; Volume 2, pp. 1178–1183.
12. Eilts, L.E.; Schleif, F.R. Governing features and performance of the first 600-MW hydrogenerating unit at grand coulee. *IEEE Trans. Power Appar. Syst.* **1977**, *96*, 457–466. [[CrossRef](#)]
13. Filbert, T.L.; Wozniak, L. Speed loop cancellation governor for hydrogenerators. II. Application. *IEEE Trans. Energy Convers.* **1988**, *3*, 91–94. [[CrossRef](#)]
14. Lim, C.M. A self-tuning stabiliser for excitation or governor control of power systems. *IEEE Trans. Energy Convers.* **1989**, *4*, 152–159. [[CrossRef](#)]
15. Lansberry, J.E.; Wozniak, L.; Goldberg, D.E. Optimal hydrogenerator governor tuning with a genetic algorithm. *IEEE Trans. Energy Convers.* **1992**, *7*, 623–630. [[CrossRef](#)]
16. Yamamoto, T.; Kaneda, M.; Oki, T.; Watanabe, E.; Tanaka, K. Intelligent tuning PID controllers. In Proceedings of the 1995 IEEE International Conference on Systems, Man and Cybernetics. Intelligent Systems for the 21st Century, Vancouver, BC, Canada, 22–25 October 1995; Volume 3, pp. 2610–2615.
17. Padrón, S.; Hernández, M.; Falcón, A. Reducing Under-Frequency Load Shedding in Isolated Power Systems Using Neural Networks. Gran Canaria: A Case Study. *IEEE Trans. Power Syst.* **2016**, *31*, 63–71. [[CrossRef](#)]
18. Venayagamoorthy, G.K.; Harley, R.G.; Wunsch, D.C. Implementation of adaptive critic-based neurocontrollers for turbogenerators in a multimachine power system. *IEEE Trans. Neural Netw.* **2003**, *14*, 1047–1064. [[CrossRef](#)] [[PubMed](#)]
19. Natarajan, K. Robust PID Controller Design for Hydroturbines. *IEEE Trans. Energy Convers.* **2005**, *20*, 661–667. [[CrossRef](#)]
20. Fangle, Q.; Guo, W. Robust H $\infty$  control for hydro-turbine governing system of hydropower plant with super long headrace tunnel. *Electr. Power Energy Syst.* **2021**, *124*, 106336.
21. Liu, Y.; Guo, W. Multi-frequency dynamic performance of hydropower plant under coupling effect of power grid and turbine regulating system with surge tank. *Renew. Energy* **2021**, *171*, 557–581. [[CrossRef](#)]
22. Xu, X.; Guo, W. Chaotic behavior of turbine regulating system for hydropower station under effect of nonlinear turbine characteristics. *Sustain. Energy Technol. Assess.* **2021**, *44*, 101088.
23. Mahdi, M.M.; Mhawi Thajeel, E.; Ahmad, A.Z. Load Frequency Control for Hybrid Micro-grid Using MRAC with ANN Under-sudden Load Changes. In Proceedings of the 2018 Third Scientific Conference of Electrical Engineering (SCEE), Baghdad, Iraq, 19–20 December 2018; pp. 220–225.

24. Kishor, N.; Saini, R.P.; Singh, S.P. A review on Hydropower Plant Models and Control. *Renew. Sustain. Energy Rev.* **2007**, *11*, 776–796. [[CrossRef](#)]
25. Ramey, D.G.; Skooglund, J.W. Detailed Hydrogovernor Representation for System Stability Studies. *IEEE Trans. Power Appar. Syst.* **1970**, *PAS-89*, 106–112. [[CrossRef](#)]
26. Mover, Working Group Prime, and Energy Supply. Hydraulic turbine and turbine control models for system dynamic studies. *IEEE Trans. Power Syst.* **1992**, *7*, 167–179. [[CrossRef](#)]
27. IEEE. Guide for the Application of Turbine Governing Systems for Hydroelectric Generating Units. In *IEEE Std 1207-2004*; IEEE: New York, NY, USA, 2004; pp. 1–140. [[CrossRef](#)]
28. Murat, D.; Kosalay, I.; Gezer, D.; Sahin, C. Validation of hydroelectric power plant model for speed governor development studies. In Proceedings of the 2015 International Conference on Renewable Energy Research and Applications (ICRERA), Palermo, Italy, 22–25 November 2015; pp. 278–282.
29. Piriz, H.D.; Cannatella, A.R.; Guerra, E.; Porcari, D.A. Inertia of Hydrogenerators, Influence on the Dimensioning, Cost, Efficiency and Performance of the Units. In Proceedings of the CIGRE Paris Session, Paris, France, 27–31 August 2012; pp. A1–A102.
30. Fischer, N.; Benmouyal, G.; Samineni, S. Tutorial on the Impact of the Synchronous Generator Model on Protection Studies. In Proceedings of the 35th Annual Western Protective Relay Conference, Spokane, WA, USA, 20–22 October 2008.
31. Kundur, P. *Power System Stability and Control*; McGraw-Hill: New York, NY, USA, 1994.
32. Report, IEEE Committee. Computer representation of excitation systems. *IEEE Trans. Power Appar. Syst.* **1968**, *PAS-87*, 1460–1464. [[CrossRef](#)]
33. Vournas, C.D.; Papaioannou, G. Modelling and stability of a hydro plant with two surge tanks. *IEEE Trans. Energy Convers.* **1995**, *10*, 368–375. [[CrossRef](#)]
34. Munoz-Hernandez, G.A. *Modelling and Controlling Hydropower Plants*; Springer: New York, NY, USA, 2013.
35. Cebeci, M.E. The Effects of Hydro Power Plants' Governor Settings on the Stability of Turkish Power System Frequency. Master's Thesis, Middle East Technical University, Ankara, Turkey, 2009.
36. Landau, I.D.; Lozano, R.; M'Saad, M.; Karimi, A. *Adaptive Control: Algorithms, Analysis and Applications*; Springer: New York, NY, USA, 2011.
37. Lavretsky, E. Adaptive control: Introduction, overview, and applications. In Proceedings of the NASA Adaptive Control Workshop, NASA Marshall Space Center, Huntsville, AL, USA, 17–20 March 2009.
38. Ioannou, P.A. *Robust Adaptive Control*; PTR Prentice-Hall: New York, NY, USA, 1996.
39. Sevcik, K. Model Reference Adaptive Control MRAC Tutorial. Available online: <http://www.pages.drexel.edu/~jkws23/tutorials/MRAC/MRAC.html> (accessed on 15 November 2016).
40. Astrom, K.J.; Wittenmark, B. *Adaptive Control*, 2nd ed.; Addison-Wesley Longman Publishing Co., Inc.: Boston, MA, USA, 1994.
41. Perdukova, D.; Fedor, P.; Fedak, V.; Padmanaban, S. Lyapunov Based Reference Model of Tension Control in a Continuous Strip Processing Line with Multi-Motor Drive. *Electronics* **2019**, *8*, 60. [[CrossRef](#)]
42. Oltean, S.E.; Dulau, M.; Duka, A.V. Model Reference Adaptive Control Design for Slow Processes. A Case Study on Level Process Control. *Procedia Technol.* **2016**, *22*, 629–636. [[CrossRef](#)]
43. NERC. *North American Electric Reliability Corporation, Balancing and Frequency Control*; NERC: Princeton, NJ, USA, 2011.
44. UCTE. *Union for the Coordination of the Transmission of Electricity, UCTE Operation Handbook*; UCTE: Brussels, Belgium, 2004.
45. Energy Market Regulatory Authority, Regulation Concerning Electricity Network. Available online: <https://www.epdk.gov.tr/Detay/Icerik/3-6730/elektrik--sebeke-.html> (accessed on 15 February 2021).